Nonlinear Photoluminescence Excitation Spectroscopy of Carbon Nanotubes: Exploring the Upper Density Limit of One-Dimensional Excitons

Yoichi Murakami[1,2] and Junichiro Kono[1,*]

[1]*Department of Electrical and Computer Engineering, Rice University, Houston, Texas 77005, USA*
[2]*Department of Chemical System Engineering, University of Tokyo, Bunkyo-ku, Tokyo 113-8656, Japan*

(Received 18 April 2008; published 21 January 2009)

We have observed that photoemission from single-walled carbon nanotubes saturates in intensity as the excitation intensity increases. Each emission peak arising from specific-chirality tubes exhibited a saturation value independent of the excitation wavelength, suggesting an upper limit on the exciton density for each nanotube species. We developed a model based on diffusion-limited exciton-exciton annihilation, which allowed us to estimate exciton densities in the saturation regime. The estimated densities were found to be still substantially smaller than the expected Mott density.

DOI: 10.1103/PhysRevLett.102.037401 PACS numbers: 78.67.Ch, 71.35.−y, 78.55.−m

Optical processes in 1D semiconductors are affected by strong Coulomb interactions and have been the subject of many theoretical [1–4] and experimental [5–11] studies. Early studies of lasing in semiconductor quantum wires [5,6] stimulated much interest in the properties of *high-density* 1D excitons, or correlated electron-hole (*e-h*) pairs, especially in their stability against biexciton formation, band-gap renormalization, and dissociation. Although it has been established that excitons in quantum wires are stable up to very high densities (10^5–10^6 cm^{-1}), unanswered questions remain. An insulating exciton gas is expected to become unstable at high densities and eventually transform into a metallic *e-h* plasma at the Mott density, where the interexciton distance approaches the exciton size. At what density gain should appear and whether a clear Mott transition exists in 1D systems are open questions [2–4,7–11].

Single-walled carbon nanotubes (SWNTs) [12] have recently emerged as novel 1D solids. The exciton binding energies reported for semiconducting SWNTs are very large (~400 meV [13,14]) compared to typical GaAs quantum wires (~20 meV [2,6]). Despite much recent progress in understanding their basic optical properties, only a limited number of studies have been performed under the condition of high carrier or exciton densities [15–17]. In particular, there have been no reports quantifying exciton densities in relation to the Mott density.

Here we describe detailed characteristics of photoluminescence (PL) and photoluminescence excitation (PLE) spectra of SWNTs at high exciton densities. Although PL intensity rapidly saturated with increasing pump fluence, PL spectra were stable, indicating that there is no band-gap renormalization, screening, or dissociation into an *e-h* plasma. However, we observed *broadening and eventual complete flattening of PLE spectra* at high laser intensities. We show that this originates from strong exciton-exciton annihilation (EEA) that provides an upper limit for the exciton population in the lowest-energy (E_{11}) state. Our model, taking into account exciton diffusion in EEA, allowed us to estimate exciton densities from the saturation curves. The estimated densities for the highly saturated regime were on the order of 1×10^5 cm^{-1}, which is more than 1 order of magnitude smaller than the expected Mott density and explains the observed stability of PL spectra in the saturation regime.

The sample was prepared by ultrasonicating CoMoCAT SWNTs in D_2O with 1 wt % sodium cholate for 1 h, followed by ultracentrifugation at 111 000 g for 4 h. Only the upper 50% of the supernatant was collected. Through this procedure, SWNT bundles were effectively removed. The solution was held in a 1-mm-thick quartz cuvette. The optical density in the E_{22} region was below 0.2, which helped avoid inhomogeneous excitation and reabsorption of PL. Our tunable excitation source was a 1 kHz, ~250 fs optical parametric amplifier (OPA) pumped by a chirped pulse amplifier (Clark-MXR, CPA2010). The OPA beam was focused onto the sample with a spot size of 300–400 μm.

Figure 1(a) compares two PL spectra. The black solid curve was taken with the OPA tuned to 654 nm (or 1.90 eV) with pulse energy ≈ 29 nJ, while the red dotted curve was obtained using a weak (100 μW) cw laser with a wavelength of 658 nm. It is seen that the relative intensities of different PL peaks [labeled by their chiral vectors (n, m)] are drastically different between the two curves. The inset confirms that the two spectra coincide accurately when the OPA pulse energy is kept low (300 pJ). Figure 1(b) shows PL spectra for pulse energies of 1 nJ (curves 1 and 7), 4 nJ (2 and 6), 10 nJ (3 and 5), and 30 nJ (4). The (7,5) peak is dominant at low fluences while the (6,5) peak becomes dominant at high fluences. It is important to note that the different curves were taken in the order of no. 1 to no. 7. The near coincidence of the pair of curves at 1, 4, and 10 nJ demonstrates that the observed changes are reproducible and are not caused by any laser-induced permanent change in the sample. We also reproduced a similar power dependence in a dried film, showing that the power dependent

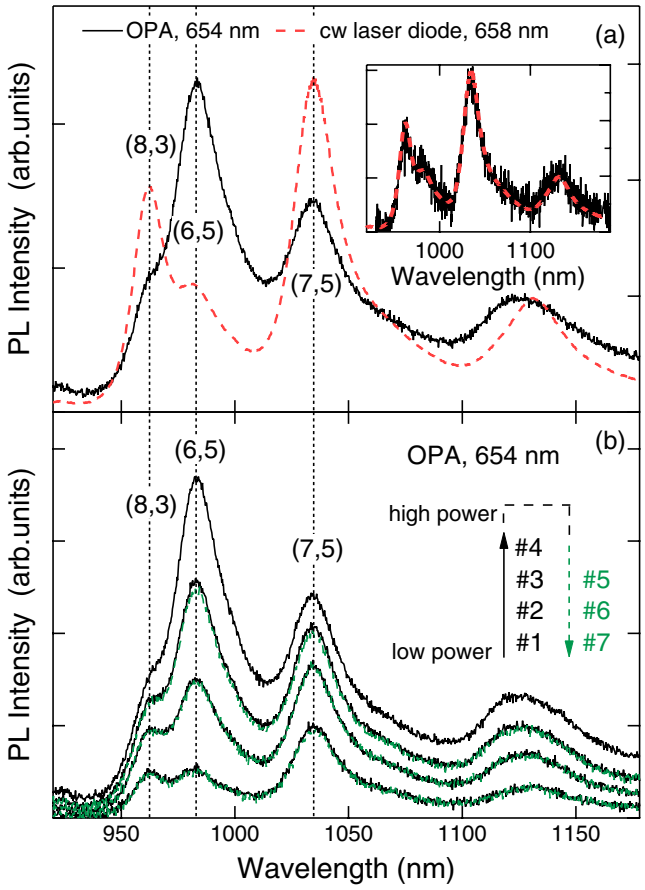

FIG. 1 (color online). Pump-intensity-dependent PL spectra. (a) Black solid curve: spectrum obtained with OPA (654 nm, 29 nJ). Red dashed curve: spectrum obtained with a cw laser diode (658 nm, 100 μW). Inset shows that the two spectra coincide when the OPA pulse energy is very low (300 pJ). (b) Change of PL spectra versus OPA pulse energy between 1 and 30 nJ (in the order of no. 1 to no. 7). Curve 4 corresponds to the highest fluence ($\sim 1.3 \times 10^{14}$ photons/cm^2).

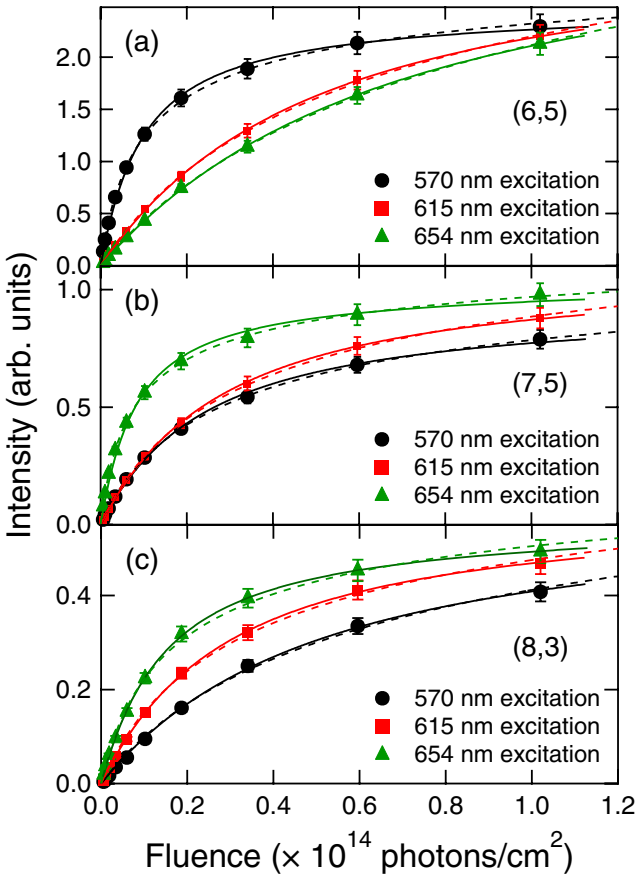

FIG. 2 (color online). Integrated PL intensity versus pump fluence for (6,5), (7,5), and (8,3) SWNTs. Pump wavelengths were 570 nm (circles), 615 nm (squares), and 654 nm (triangles). The error bars account for $\pm 5\%$. The solid curves and the dashed curves are fitting by Eq. (3) and (4), respectively.

changes are not an artifact caused by the fluidic nature of the sample. Finally, note that the PL intensities tend to saturate at high laser fluences, while their peak positions do not change at all and linewidths increase only slightly (by $\sim 15\%$ from curve 1 to 4).

Figures 2(a)–2(c) plot integrated PL intensities for (6,5), (7,5), and (8,3) tubes, respectively, versus pump fluence with pump wavelengths of 570, 615, and 654 nm. The E_{22}-resonant wavelengths of these tube types are 570, 647, and 673 nm, respectively. The integrated PL intensities were obtained through spectral decomposition assuming 50% Lorentzian + 50% Gaussian, while keeping the peak positions fixed. Figure 2 indicates that saturation starts at a lower (higher) fluence when the sample is resonantly (nonresonantly) excited. The unexpectedly fast saturation of the (7,5) peak with 570 nm excitation (which is nonresonant) is likely due to its proximity to the phonon sideband at 585 nm [18]. The solid curves and the dashed curves are theoretical fits to the experimental curves based on our model to be discussed later.

Figures 3(a)–3(d) show PLE maps taken with various pump fluences. The step size for the pump photon energy was 20 meV. The lowest fluence data [Fig. 3(a)] is essentially the same as that taken with low-intensity cw light. However, as the fluence is increased [Figs. 3(b)–3(d)], the E_{22} excitation peaks gradually broaden and eventually become completely flat at the highest fluence (1.2×10^{14} photons/cm^2); i.e., *PL intensities become independent of the excitation wavelength*. The corresponding PLE spectra are shown in Figs. 3(e)–3(h) for three PL wavelengths at 983, 1034, and 1125 nm.

To provide further insight into the nature of the observed broadening and flattening of PLE spectra, we performed absorption measurements in the E_{22} region using OPA pulses. Figure 4 compares two transmission spectra measured with fluences of 1.0×10^{12} photons/cm^2 (linear regime) and 1.0×10^{14} photons/cm^2 (saturation regime), respectively, and a transmission spectrum taken with weak cw white light. It is clear from the figure that the E_{22} absorption peaks do not exhibit any broadening and shifts even in the saturation regime, strongly suggesting that

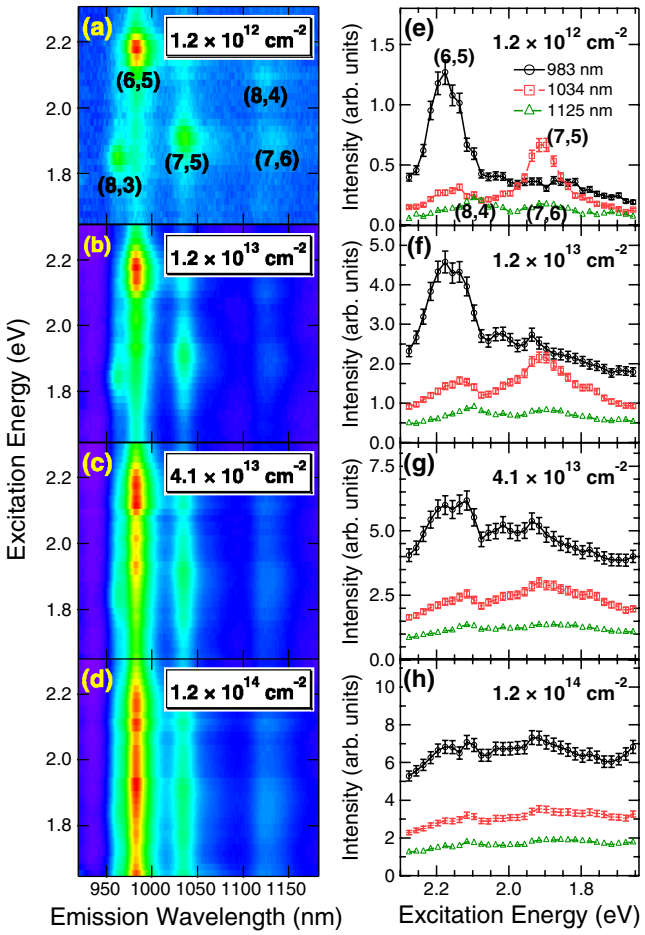

FIG. 3 (color online). Evolution of PLE data with increasing pump fluence: (a) 1.2×10^{12}, (b) 1.2×10^{13}, (c) 4.1×10^{13}, and (d) 1.2×10^{14} photons/cm^2. (e)–(h) PLE spectra corresponding to (a)–(d) at PL wavelengths of 983 nm (circles), 1034 nm (squares), and 1125 nm (triangles). The magnitude of experimental error for the 1125 nm case is comparable to or slightly smaller than the size of the triangle marks.

these intensities are not high enough to cause light-induced nonlinear effects such as state (or phase-space) filling on states in the E_{22} range.

We interpret these observations as results of very efficient EEA [17,19]. We assume that the formation of E_{11} excitons occurs in a very short time scale (e.g., ~40 fs [20]), shorter than our pulse width (~250 fs). Thus, they accumulate in E_{11} during and right after photocreation of e-h pairs. However, the number of excitons that can be accommodated in the E_{11} state is limited by EEA. As the exciton density n_x approaches its maximum value, EEA begins to prevent a further increase by efficiently removing excitons nonradiatively, explaining the PL saturation. Since EEA serves as a bottleneck for the exciton density, the PL intensity becomes insensitive to whether the excitons were created resonantly or nonresonantly and independent of the pump wavelength. Namely, at very high pump fluences, the PL intensity is determined not by how efficiently excitons are created but by *how many* E_{11} *excitons can be accommodated within a particular type of SWNT* as well as by the relative abundance of that type of SWNT in the sample.

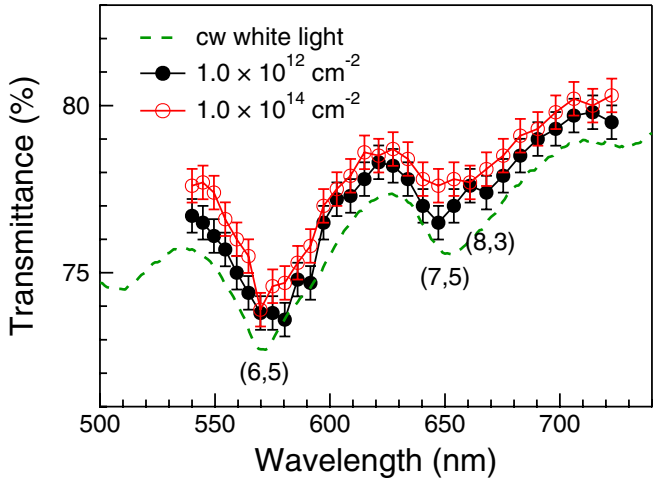

FIG. 4 (color online). Transmission spectra measured with high-fluence OPA pulses (filled circles, 1.0×10^{12} photons/cm^2; open circles, 1.0×10^{14} photons/cm^2) compared with a transmission spectrum taken with a weak cw white-light beam (dashed line).

We have developed a model to deduce exciton densities n_x from the PL saturation curves. Existing EEA models [17,19] assume an annihilation rate $\propto n_x^2$, a probability of finding two excitons at the same position. However, its validity becomes questionable when one deals with high-density excitons in 1D where the dynamics and/or size of the excitons are expected to influence the annihilation rate. We introduce a dimensionless exciton population ($0 \leq \zeta < 1$) defined as $\zeta \equiv N l_x / L$, where N is the number of excitons in a SWNT, L is the SWNT length, and l_x is the characteristic length scale each exciton "occupies" in the SWNT. In a static limit, l_x should simply be the exciton size. However, recent experiments have indicated the importance of exciton *diffusion* [21–23]. In particular, Cognet *et al.* [23], via micro-PL studies on single micelle-suspended SWNTs of various chiralities, found that excitons diffusively traverse a substantial distance (~90 nm) within their lifetime. Therefore, we assume that l_x is determined by the diffusion length and any two excitons formed within l_x undergo EEA.

The essence of our model is described as follows (the complete details and validations are given in Ref. [24]): A 1D space of length L is considered where N segments of length l_x have populated without overlapping each other (i.e., $N l_x < L$). The probability for a new segment (of length l_x) entering the system *not* to overlap with any of the N existing segments, $p(N)$, is given by

$$p(N) = \left(1 - \frac{N l_x}{L}\right)\left(1 - \frac{l_x}{L - N l_x}\right)^N. \quad (1)$$

We also assume that an exciton promoted to a higher energy level as a result of EEA returns to the E_{11} level

with 100% probability due to ultrafast and efficient E_{22}-to-E_{11} relaxation; i.e., two excitons become one exciton through EEA. In this case, the expectation value of the increment of N by the addition of the new segments, $\langle \Delta N \rangle_N$, is equal to $p(N)$ in Eq. (1). Therefore, in the *instantaneous limit* where the initial creation of excitons occurs within a very short time before EEA follows, the relationship between the number of initially created excitons N_0 and resultant N is described by a differential equation of $dN_0/dN = 1/\langle \Delta N \rangle_N$ $[= 1/p(N)]$.

This differential equation, based on $N \propto I_{\mathrm{PL}} \equiv c_1 \zeta$ and $N_0 \propto I_{\mathrm{pump}} \equiv c_2 \psi$ (c_1, c_2, coefficients; I_{PL}, I_{pump}, PL and pump intensities), is expressed with ζ and ψ as

$$\frac{d\psi}{d\zeta} = \frac{1}{(1-\zeta)\{1 - \frac{l_x}{L}(1-\zeta)^{-1}\}^{(L/l_x)\zeta}}. \quad (2)$$

The Taylor expansion of the denominator of Eq. (2) and elimination of higher-order terms of l_x/L result in a differential equation of only ζ and ψ. Finally, the integration yields the solution for the instantaneous limit as

$$\psi = \frac{1}{e}\left\{\mathrm{Ei}\left(\frac{1}{1-\zeta}\right) - \mathrm{Ei}(1)\right\}, \quad (3)$$

and similarly, the solution for the *steady-state limit* corresponding to cw excitation [24] is obtained as

$$\psi = \frac{\zeta}{1-\zeta}\exp\left(\frac{\zeta}{1-\zeta}\right) \qquad \left[\zeta \equiv \frac{I_{\mathrm{PL}}}{c_1},\ \psi \equiv \frac{I_{\mathrm{pump}}}{c_2}\right]. \quad (4)$$

The actual experimental situation is somewhere between those two limits but closer to the former. Equations (3) and (4) are implicit equations relating I_{PL} and I_{pump} in terms of their respective dimensionless parameters, ζ and ψ. They contain no fitting parameters other than the two linear scaling factors c_1 and c_2 and simply become a linear relationship ($\psi = \zeta$) in the low density limit ($\zeta \to 0$).

The solid curves and the dashed curves in Fig. 2 are fits to the data by Eqs. (3) and (4), respectively, showing good agreement. The values of ζ were obtained through this analysis for respective data points shown in Fig. 2. Finally, the exciton density can be obtained through $n_x = \zeta/l_x$. Using $l_x = 45$ nm (one half of the excursion range defined in [23]), we estimated n_x for (6,5) to be 1.7×10^5, 1.3×10^5, and 1.1×10^5 cm^{-1} for excitation with 570, 615, and 654 nm, respectively, at a fluence of 1.02×10^{14} photons/cm^2 in the instantaneous limit. These densities are still much smaller than the expected Mott density n_x^* ($\sim 7 \times 10^6$ cm^{-1}, assuming exciton size $\sim$1.5 nm [25]), which can explain the stability of PL (Fig. 1) in the saturated regime. On the other hand, the densities of *as-created e-h* pairs before undergoing EEA are estimated to be 1–2 $\times 10^6$ cm^{-1} in the cases of resonant excitation, which is similar to n_x^*. These observations appear qualitatively different from GaAs quantum wires where PL saturation is not obvious until the formation of biexcitons and an *e-h* plasma [11]. Highly efficient *and* rapid EEA in SWNTs, which is consistent with the reported absence of biexciton signatures [26], is probably the direct reason for such characteristic differences.

In summary, we have studied PL and PLE spectra of SWNTs at high exciton densities. Complete flattening of PLE spectra and clear PL saturation were observed, indicating the existence of an upper density limit. We developed a model that reproduced the observed saturation behavior and allowed us to estimate exciton densities, which remained more than 1 order of magnitude lower than the expected Mott density and explained the stability of PL spectra in the saturated regime.

We thank the Robert A. Welch Foundation (C-1509) and NSF (DMR-0325474 and OISE-0530220) for support and H. Akiyama, K. Matsuda, and A. Srivastava for valuable discussions. One of us (Y. M.) was supported by JSPS (18-09883) and thanks T. Okubo and S. Maruyama for their support.

*Corresponding author.
kono@rice.edu

[1] T. Ogawa and T. Takagahara, Phys. Rev. B **43**, 14325 (1991); **44**, 8138 (1991).
[2] F. Rossi and E. Molinari, Phys. Rev. Lett. **76**, 3642 (1996).
[3] F. Tassone and C. Piermarocchi, Phys. Rev. Lett. **82**, 843 (1999); C. Piermarocchi and F. Tassone, Phys. Rev. B **63**, 245308 (2001).
[4] S. Das Sarma and D. W. Wang, Phys. Rev. Lett. **84**, 2010 (2000); D. W. Wang and S. Das Sarma, Phys. Rev. B **64**, 195313 (2001).
[5] E. Kapon *et al.*, Phys. Rev. Lett. **63**, 430 (1989).
[6] W. Wegscheider *et al.*, Phys. Rev. Lett. **71**, 4071 (1993).
[7] R. Ambigapathy *et al.*, Phys. Rev. Lett. **78**, 3579 (1997).
[8] J. Rubio *et al.*, Solid State Commun. **120**, 423 (2001).
[9] H. Akiyama *et al.*, Phys. Rev. B **67**, 041302 (2003).
[10] T. Guillet *et al.*, Phys. Rev. B **67**, 235324 (2003).
[11] Y. Hayamizu *et al.*, Phys. Rev. Lett. **99**, 167403 (2007).
[12] S. Iijima and T. Ichihashi, Nature (London) **363**, 603 (1993).
[13] F. Wang *et al.*, Science **308**, 838 (2005).
[14] J. Maultzsch *et al.*, Phys. Rev. B **72**, 241402 (2005).
[15] F. Wang *et al.*, Phys. Rev. B **70**, 241403 (2004).
[16] G. N. Ostojic *et al.*, Phys. Rev. Lett. **94**, 097401 (2005).
[17] Y.-Z. Ma *et al.*, Phys. Rev. Lett. **94**, 157402 (2005).
[18] Y. Miyauchi and S. Mauyama, Phys. Rev. B **74**, 035415 (2006).
[19] T. W. Roberti *et al.*, J. Chem. Phys. **108**, 2143 (1998).
[20] C. Manzoni *et al.*, Phys. Rev. Lett. **94**, 207401 (2005).
[21] C.-X. Sheng *et al.*, Phys. Rev. B **71**, 125427 (2005).
[22] R. M. Russo *et al.*, Phys. Rev. B **74**, 041405 (2006).
[23] L. Cognet *et al.*, Science **316**, 1465 (2007).
[24] Y. Murakami and J. Kono, arXiv:0901.0211v1.
[25] V. Perebeinos *et al.*, Phys. Rev. Lett. **92**, 257402 (2004).
[26] K. Matsuda *et al.*, Phys. Rev. B **77**, 033406 (2008).